

MEDICAL ROBOTS

Using the fringe field of a clinical MRI scanner enables robotic navigation of tethered instruments in deeper vascular regions

Arash Azizi, Charles C. Tremblay, Kévin Gagné, Sylvain Martel*

Copyright © 2019
The Authors, some
rights reserved;
exclusive licensee
American Association
for the Advancement
of Science. No claim
to original U.S.
Government Works

Navigating tethered instruments through the vasculatures to reach deeper physiological locations presently inaccessible would extend the applicability of many medical interventions, including but not limited to local diagnostics, imaging, and therapies. Navigation through narrower vessels requires minimizing the diameter of the instrument, resulting in a decrease of its stiffness until steerability becomes unpractical, while pushing the instrument at the insertion site to counteract the friction forces from the vessel walls caused by the bending of the instrument. To reach beyond the limit of using a pushing force alone, we report a method relying on a complementary directional pulling force at the tip created by gradients resulting from the magnetic fringe field emanating outside a clinical magnetic resonance imaging (MRI) scanner. The pulling force resulting from gradients exceeding 2 tesla per meter in a space that supports human-scale interventions allows the use of smaller magnets, such as the deformable spring as described here, at the tip of the instrument. Directional forces are achieved by robotically positioning the patient at predetermined successive locations inside the fringe field, a method that we refer to as fringe field navigation (FFN). We show through *in vitro* and *in vivo* experiments that x-ray-guided FFN could navigate microguidewires through complex vasculatures well beyond the limit of manual procedures and existing magnetic platforms. Our approach facilitated miniaturization of the instrument by replacing the torque from a relatively weak magnetic field with a configuration designed to exploit the superconducting magnet-based directional forces available in clinical MRI rooms.

INTRODUCTION

The scope of catheter guidewire-based procedures is broadening, and endovascular access is reshaping medical treatments through less invasive operations. Catheters are used in endovascular interventions for minimally invasive treatments of various vascular diseases (1). Interventional oncology has introduced tumor treatment techniques relying on the catheterization of the arteries that supply blood to the tumor to either block the blood vessels or inject the drug near the tumor (2, 3). In interventional cardiology, catheters are used for minimal invasive operation inside the heart for diagnosis or treatment purposes (4).

In the domain of endovascular interventions, the need to access locations deeper inside the vascular system is growing. Recent advances in developing untethered milli-, micro-, and nanoscale robots to perform local diagnosis and treatment inside the body, including nonsystemic drug delivery, are promising (5–15) and could take advantage of being injected closer to the target physiological location for deeper release into the vascular network. Decreasing the diameter of the guidewire used in catheterization is essential to reach deeper physiological targets through narrower vessels. However, it leads to insufficient rigidity or stiffness of the guidewire, making steerability by an operator located outside the body more difficult while requiring more trials and errors under fluoroscopy, which increases the elapsed time of the procedure. Longer procedures caused by trials and errors also expose the medical crew and the patient to increased doses of x-ray radiation, which are harmful (16–18). In the course of a procedure of catheterization and advancing the guidewire through the tortuous vascular trajectories, the friction

forces against the instruments are amplified by the added surface in contact against the vessel walls caused by the bending of the instrument. Because the overall diameter of the instrument needs to be decreased further to allow passage through narrower vessels, manual catheterization by steerability and pushing the instrument from the insertion site to reach deeper physiological locations become impossible.

To compensate for the fact that acquiring the necessary skills is a relatively long process that relies on the experience of the practitioner (19, 20), medical robotics aims to improve the efficacy of different medical interventions with different levels of autonomy (21). This is also true for robotic catheterization, which has been investigated for years to facilitate endovascular procedures with different systems (e.g., Sensei X and Magellan, Hansen Medical) with U.S. Food and Drug Administration (FDA) and/or Conformité Européenne (CE) approval for clinical use to perform specific interventions under the control of an operator (22–25), especially for applications in cardiology (7, 26, 27). Magnetism has also been exploited for this purpose. Magnetic navigation systems such as the Stereotaxis Niobe (28), Catheter Guidance Control and Imaging (Magnetecs) (29), and Aeon Phocus (Aeon) (30) rely on permanent magnets or electromagnets to generate magnetic fields, and extensive work has been done on the modeling and control of magnetic catheters using these systems (31–35). The use of a guidewire with a soft distal section can improve the maneuverability of the tip of the instrument (5). However, when the overall diameter of the instrument is reduced to penetrate narrower vessels, its stiffness reduces to a point where pushing the instrument is no longer possible. A proposed solution is applying a pulling force on the tip; hence, a directional magnetic gradient can be used to provide such a force while steering the guidewire (36) deeper (37). In (36), it was shown that a pulling force applied to the tip of a guidewire could be used for selective steering of microguidewires. Magnetic actuation was provided by integrating additional gradient

Nanorobotics Laboratory, Department of Computer and Software Engineering, Institute of Biomedical Engineering, Polytechnique Montréal, Montréal, QC, Canada.
*Corresponding author. Email: sylvain.martel@polymtl.ca

coils inside the magnetic resonance imaging (MRI) bore to generate a directional magnetic gradient of 0.5 T/m. However, installing the additional coils inside the tunnel of an MRI scanner prevents such a technology from application to a human's size, and the strong uniform magnetic field (B_0) inside the tunnel complicates the task by always inducing a strong torque along the longitudinal axis of the tunnel. Hence, fringe field navigation (FFN) (37) was introduced to exploit the strong gradients (about 2 T/m in a space that supports human-scale intervention), resulting from the fast decayed magnetic stray field known as the fringe field. The fringe field emanates outside a clinical MRI scanner, is produced by its superconducting magnet, and far exceeds the maximum strength of 0.2 T and gradient of 0.7 T/m reported in the literature (22, 36). Applying a torque by exploiting the magnetic field in the range of about 100 mT for steering instrument tips with relatively high stiffness has already been investigated (7, 22, 25–27, 33, 38). However, reducing the cross-sectional area of the guidewire (and so the stiffness) to target deeper regions in the vascular system leads to limitations in inserting the device deeper due to the added contact forces being applied between the vessel walls and the guidewire. As such and as mentioned earlier, the primary goal of FFN is to induce a pulling force as a complementary actuation mechanism to navigate microscale tethered instruments deeper through tortuous vascular networks or constrained physiological spaces. The best source for generating the highest pulling force on a magnetic tip is to use the gradient field resulting from the fast decay of the magnetic field (fringe field) originating from a superconducting magnet. Although a superconducting magnet alone could be used in FFN, in a clinical setting, FFN typically exploits the superconducting magnet already available in a clinical MRI scanner. Superconducting magnets provide the highest source of magnetization, but the field cannot be modulated like in the case of electromagnets. Another constraint is that superconducting magnets are bulky and cannot be practically moved around the patient. To resolve these issues, FFN relies on the proper positioning and orientation of the patient around the MRI scanner to pull the magnetic tip of an instrument such as a microguidewire toward a desired direction inside the blood vessels or other physiological spaces. The early *in vitro* study conducted with FFN demonstrated the potential of the technology without adequate positioning feedback for navigation purpose (37).

By mapping the fringe field in front of the MRI scanner to use it for navigation, this work reports the results of x-ray-guided FFN by using a table attached to a robotic arm for patient positioning. Here, FFN exploits the three-dimensional (3D) directional magnetic fringe field in a subspace in front of a clinical MRI scanner with robotic positioning to directionally pull the instrument along a planned trajectory. Before *in vivo* tests, FFN through tortuous and multibifurcation vascular routes was repeatedly carried out *in vitro* in small vessels with a diameter in the range of 1 to 2 mm. The magnetic actuation available in FFN was demonstrated to allow further insertion of the guidewire once it was not possible without pulling the tip caused by further miniaturization of the magnetic tip of the guidewire. In this study, FFN was also successfully performed *in vivo* in a swine model with a microguidewire being navigated in narrow blood vessels. The use of a deformable magnetic spring for the tip as an alternative to a solid permanent magnet tip, allowing optimization for the catheterization procedures, was also validated.

Experimental facility

The basic clinical facility for FFN includes a clinical MRI scanner and a table attached to a robotic arm for positioning a patient. The

fringe field of a closed bore MRI scanner features higher magnetic strengths and gradients compared with an open bore MRI scanner, making closed bore MRI scanners a better choice for the source of actuation in FFN (39). For the robot, adequate payload capacity was required to manipulate the patient. Our facility (Fig. 1) included a clinical MRI scanner (Skyra 3T, Siemens) and a robotic manipulator (KR300R2500, KUKA) that is in the class of Quantum Ultra with a rated payload of 300 kg. The robot was driven with electromotors and included magnetic parts in its structure. The strength of the magnetic field limits the distance that the robot can move close to the MRI scanner. A nonmagnetizable MRI-safe patient table was attached to the end effector of the robot while being compatible with a portable x-ray unit (Cios Alpha, Siemens) used for gathering positioning information of the distal tip of the inserted instrument. Because FFN operations can be done during periods when scheduled MRI sessions are not performed, maintaining the MR image quality that could be distorted by the proximity of this large robotic platform is essential. Hence, shimming of the scanner was done when the robotic arm was set to a predefined position used when FFN was not performed. In this configuration, tests showed that the full quality of MRI was maintained.

RESULTS

FFN navigates microguidewire in multibifurcation, tortuous, narrow vessels

The steps of mapping the fringe field (Fig. 2), the method, the protocol used for the FFN experiments, and the experimental procedure are described in Materials and Methods and the Supplementary Materials. In brief, the location and the direction of the vessels of a patient laid on the MRI-safe robotic patient table (see Supplementary Materials) are required data in FFN. The method is based on the robotic positioning of the table to align the direction of the vessel ahead of the point at which the tip of the guidewire is placed with the direction of the magnetic gradient force applied from the fringe field. This positioning is a composition of a 3D rotation and translation of the table. Here, we limited the pitch and roll rotation of the table to 15°. We chose this value from the configurations of a robotic patient positioning system (ORION, LEONI) that has received FDA approval and CE mark. The procedure for FFN conducted in a vascular path consists of sequences of positioning the table in the fringe field followed by feeding the guidewire through successive segments of the vessels. The system for feeding the guidewire (Fig. 3F) is described in the Supplementary Materials. The vascular model (Fig. 3A and fig. S1) used for *in vitro* experiment was made from the model of the hepatic arteries of a swine. The phantom models present physiological features for navigation through multiple bifurcations (maximum 3), tortuous paths (target T3 includes two consecutive ~90° deviation after B3, and target T5 is curved after B5 with ~180° variation in the direction of the vessel), and narrow blood vessels (in the range of 1 to 2 mm in diameter) while allowing navigation from a large vessel toward a narrow vessel at target T6 in Fig. 3 (from ~7 to ~1.5 mm in diameter).

The smallest magnet used for the tip of the microguidewire has an equivalent spherical radius of 0.416 mm. A map of the magnetic gradient force from the fringe field (see Materials and Methods) was calculated by assuming that the external magnetic field can rotate the magnetic tip of the guidewire to align its magnetization direction with the external magnetic field. The occurrence of the alignment

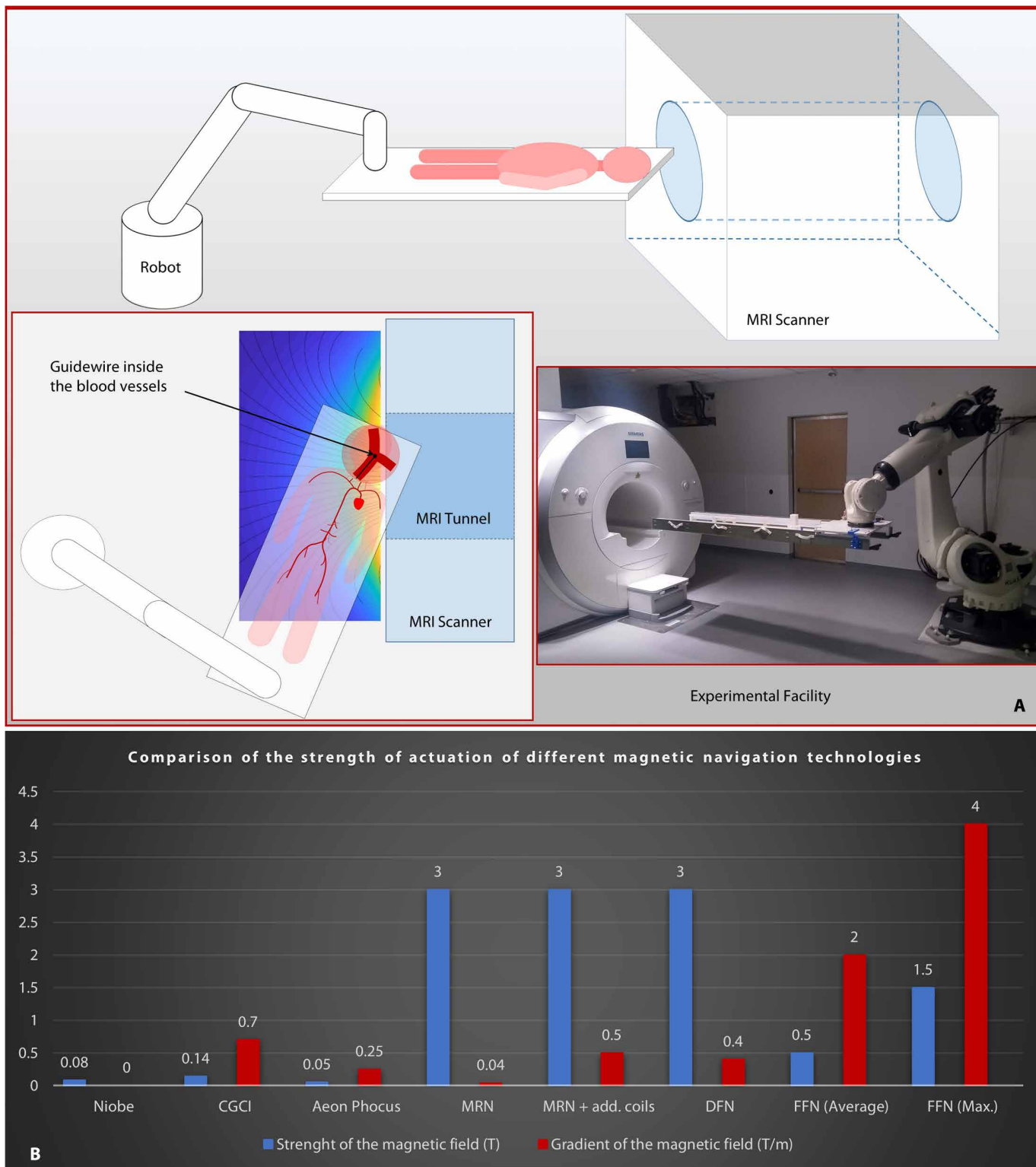


Fig. 1. The concept of FFN and comparing it with other magnetic navigation technologies. (A) Schematic of the concept of FFN and our experimental facility, and **(B)** comparison of the strength of the actuation of various magnetic navigation technologies (22, 37). MRN, magnetic resonance navigation; DFN, dipole field navigation.

was validated visually by probing the direction of the magnetic field lines and comparing it with the orientation of the tip of the guidewire inside the phantom at the zones where the strength of the external

magnetic field was ~ 0.15 T and higher. The microguidewire that we used for the experiments (see Materials and Methods) has a floppy distal with a length of 8 cm (HYBRID007D, Balt). This characteristic

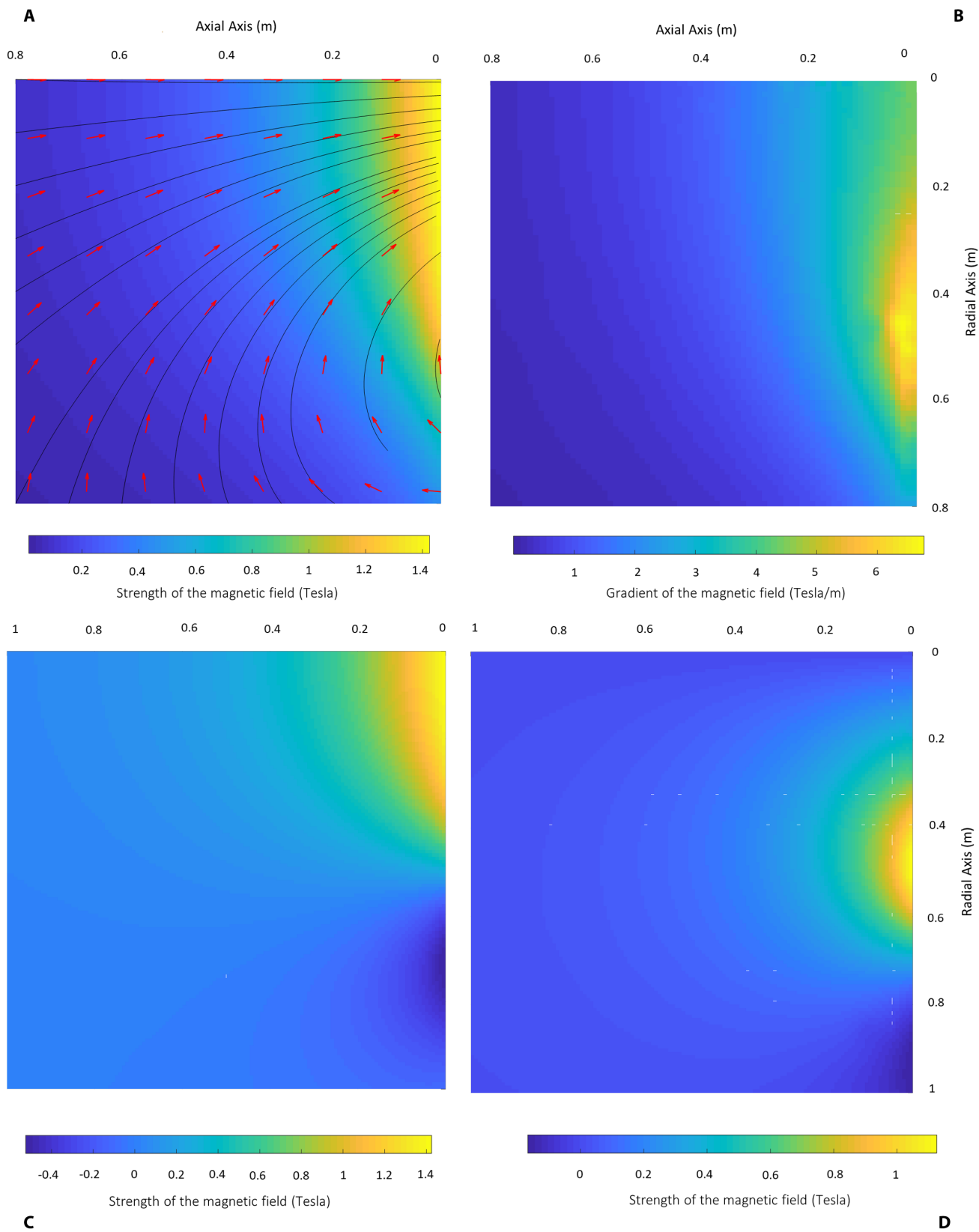


Fig. 2. Map of a radial plane of the magnetic fringe field of the MRI scanner. (A) Map of the sum of the components of the fringe field of 3T MAGNETOM Skyra. Black lines and red arrows represent the direction of the magnetic field vector. The reference of axial component is ~ 5 cm from the front face of the MRI scanner. (B) Amplitude of the directional gradient of the total magnetic field. (C) Map of the axial component and (D) map of the radial component of the fringe field.

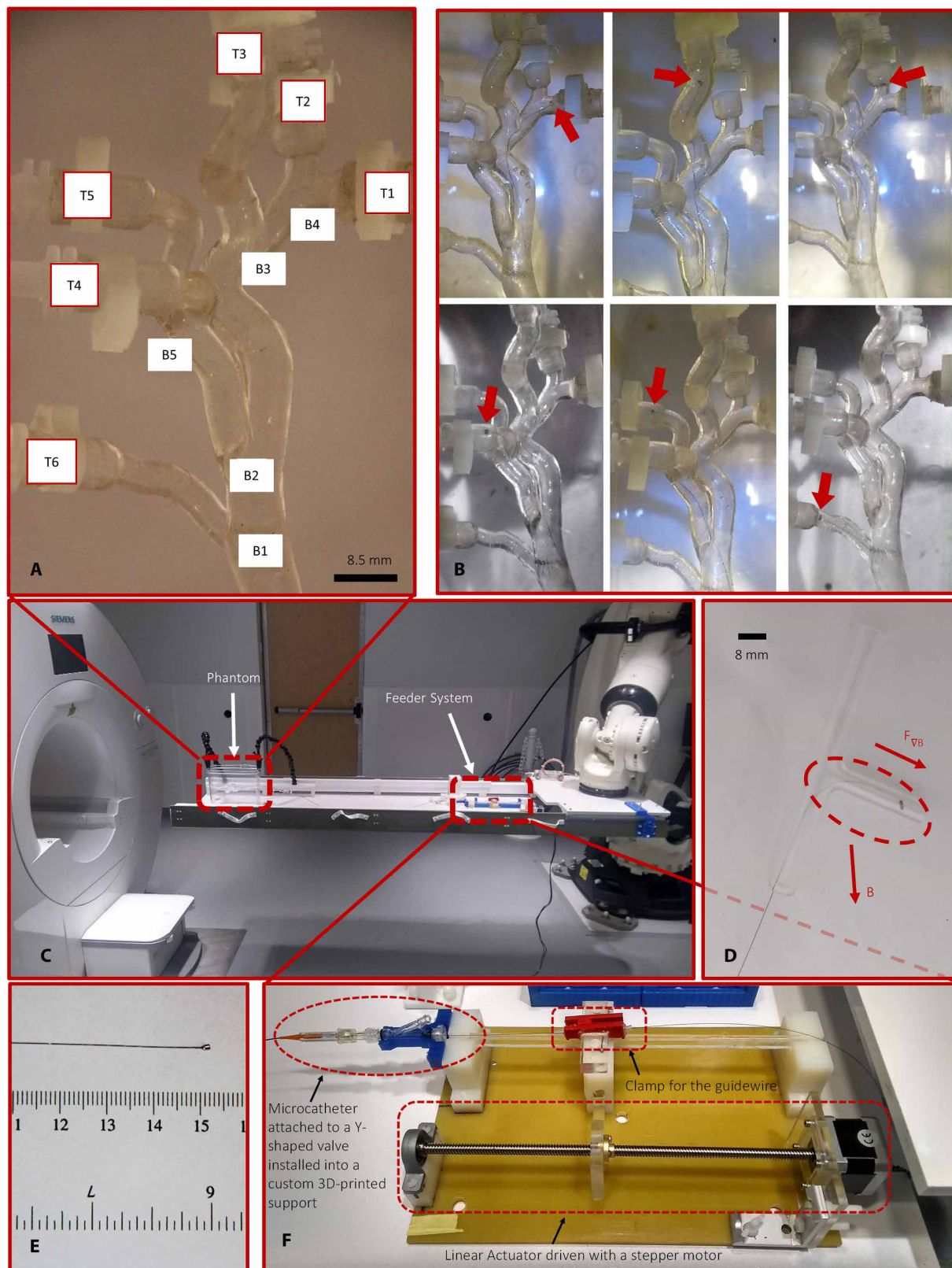


Fig. 3. Results of in vitro FFN experiments for the navigation of the magnetic microguidewire to different targets of the vascular model. (A) Phantom and its different bifurcations and targets. **(B)** Location of the tip of the guidewire (red arrow) at the end of each route. **(C)** Setup of the in vitro experiment and location of the phantom and system for feeding the guidewire. **(D)** Example of a kink occurring at the tip of the guidewire due to field gradient deviation. **(E)** Microguidewire with a magnetic tip attached at its tip (cylindrical with diameter and length of 1 mm). **(F)** System for feeding the guidewire.

of the guidewire was preferred to minimize the elastic resistance of the tip of the tether against the magnetic torque applied on the magnetic tip.

In vitro FFN experiments of navigating a microguidewire to all the targets on the vascular model were performed by defining sequences that exploited the highest available magnetic actuation. For this purpose, various experiments by exploiting different points in the map of the fringe field for each segment on the vascular path were designed. Experiments for targets 1, 2, 4, 5, and 6 were performed by sequences that exploited zones in the fringe field where the field $B > 0.5$ T and the gradient $\nabla B > 2$ T/m, with the deviation angle between the magnetic field line and the magnetic gradient force in the fringe field (field gradient deviation) being less than 20° . In our experiments, we observed that, when the field gradient deviation was more than 30° , a noticeable kink occurred at the tip of the guidewire (Fig. 3D). This kink affected the maneuverability of the tip. The reason is that the magnetic field rotates the tip to align its magnetization with the external magnetic field, while the tether is under tension by the magnetic gradient force exerted on the tip. Regarding the time of the experiments, although these figures could be improved in the future, each sequence of FFN to move the sample from a general position to the predetermined position for the FFN navigation, followed by feeding the guidewire and returning to the general position, took about 2 min, and the velocity of the robot was limited to 20 cm/s. A full experiment for navigating the guidewire through a vascular path took between 8 min on average for the shortest path (target T4) and about 20 min for the longest path (targets T3 and T5). In addition, more than five various experiments were performed for each target by using different points in the fringe field, and each experiment had been performed multiple times (three to five times).

The direction of the vessel after bifurcation 3 and toward target 3 was perpendicular to the overlay of the patient table for the way that we initially prepared the phantom and fixed it inside a box. For that section of the vessel, zones in the fringe field with a large field gradient deviation ($>45^\circ$) were used. In addition, the magnetic field strength for sequences of navigation ranged between 0.1 and 0.5 T. We consider those sequences not to be optimal situations for FFN. The success of the experiment for navigation to target 3 was low, and giving shocks to the guidewire by turning the tether along its central axis or giving slack by extra feeding facilitated inserting the guidewire. However, this section was navigated successfully by rotating the phantom and changing the direction of the vessel to define sequences of FFN that exploited stronger magnetic actuation ($B > 0.5$ T and $\nabla B > 2$ T/m). Such a change in the position of the phantom can be viewed as changing the recumbent position of the patient on the table. Figure 3B shows the final results of the experiments with the tip of the guidewire reaching each target. Sample videos of in vitro experiments are available as Supplementary Materials.

In addition, guiding the guidewire along the predefined paths was done by x-ray imaging. To perform the image-guided experiments, we placed the x-ray imaging console in the MRI room at a location where the strength of the magnetic fringe field was less than 1 mT. Examples of the cases of using the x-ray imaging for validation of the location of the tip of the guidewire throughout an FFN experiment are presented in fig. S2. Each image gathering was done at the expected position of the tip at the end of each FFN sequence by registration of the vascular trajectory (indexed data) on the x-ray image using a geometrical approach (method described in the

Supplementary Materials). The position of the tip of the guidewire was adjusted by either pulling the guidewire back (in case of passing the expected location) or repeating the previous sequence.

The importance of collision-free robotic positioning of the patient in FFN is undeniable for safety issues. Conditions that we established for robotic positioning and predicting collision were validated to be safe throughout all in vitro FFN experiments (see Supplementary Materials and Methods).

Stronger magnetic actuation in FFN allows miniaturization of the tip

In the previous set of experiments, we demonstrated the possibility of navigating a microguidewire in the vascular structures along a desired path. In a catheterization procedure, the step after placing a guidewire in a vascular branch is to insert a catheter and then remove the guidewire. An objective of FFN is to successfully navigate the guidewire in narrow blood vessels in a trade-off of miniaturizing the magnet attached to the tip of the microguidewire and using stronger gradient and strength from the fringe field. This miniaturization would enable the retrieval of the microguidewire with a rigid tip larger than its tether through a catheter with the smallest inside diameter. Decreasing the volume of the magnetic tip corresponds to weaker magnetic actuation. Here, instead of using a smaller magnetic tip, we designed FFN experiments that exploit a weaker magnetic actuation by selecting thresholds for the highest acceptable strength of the magnetic field and so the gradient of the magnetic field.

We defined sequences of FFN for all the targets on the phantom except target 3 by choosing upper thresholds for the highest admissible strength of the magnetic field. The goal was to find the lowest magnetic actuation that hinders successful navigation. For targets 1 and 2, the most challenging part was the navigation at bifurcation 3. The experiments were unsuccessful for the sequences that exploited a magnetic field in the range of 0.15 to 0.25 T, where the gradient was about 0.3 to 0.6 T/m. Adding extra bending at the tip by the magnetic field did not enable steering the guidewire into bifurcation 3 when $B \sim 0.2$ T. For target 5, navigation of the guidewire into bifurcation 5 and after that failed for sequences that exploited the strength of the magnetic field of less than 0.35 T, where the gradient is about 0.7 T/m. This threshold for target 6 was about 0.15 T. A conclusion of this experiment is the possibility of miniaturization of the magnetic tip with FFN to enable targeting smaller vessels and retrieval of the guidewire through a microcatheter.

Magnetic gradient attraction force pulls the guidewire further inside the vessel

Intermittent contacts between the guidewire and the vessel walls in the tortuous vascular structure induce resistive forces on the guidewire that affect the insertion of the guidewire. As a result, although the guidewire can be inserted from its other end outside of the body, the tip of the guidewire does not advance inside the vessel, and the distal section of the guidewire crooks. FFN is considered to provide a solution for this issue by applying a pulling force at the tip to enable further insertion of the tip of the guidewire.

In in vitro experiments, we observed that further insertion of the guidewire at each of the targets of the phantom is not possible without a pulling force (see Fig. 4, B, D, F, and G, and supplementary movies). The observation was done when the tip of the guidewire was at different targets and the phantom was away from the MRI ($B < 0.5$ mT). That is, we designed experiments to investigate the impact of a pulling

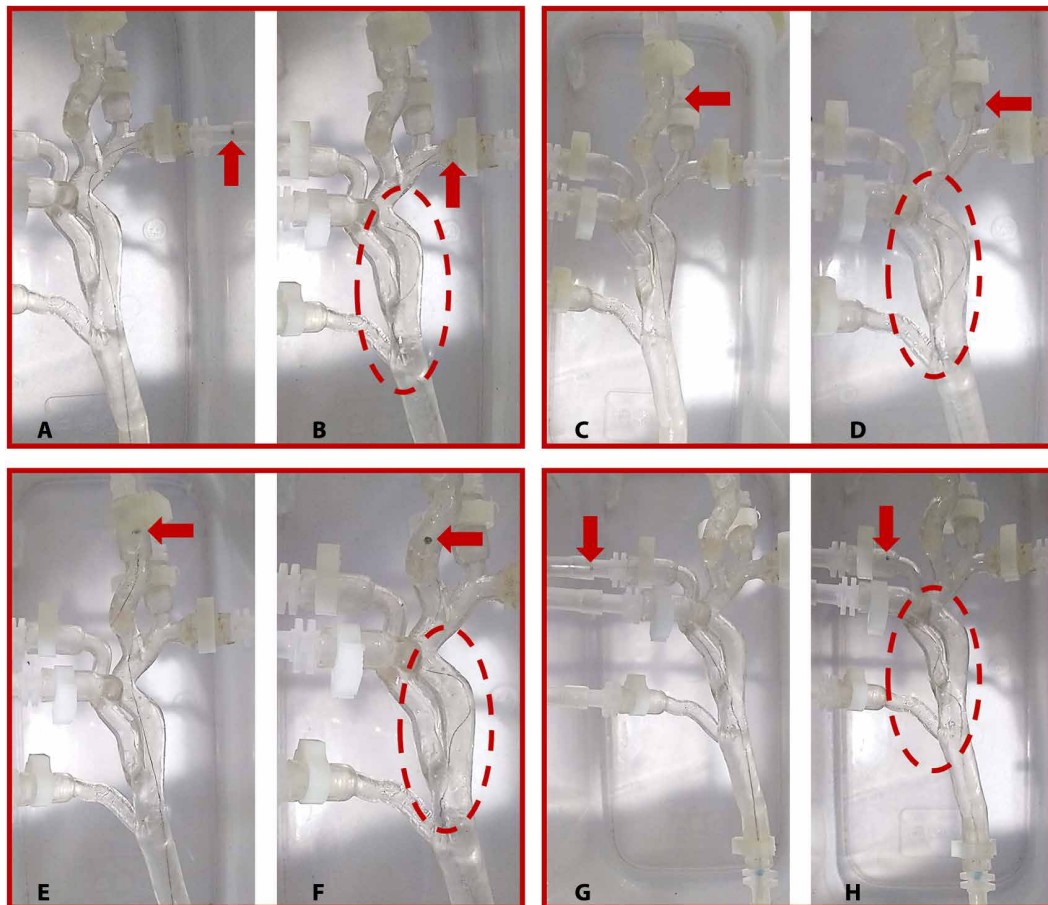


Fig. 4. Results of the FFN experiment to exploit a magnetic pulling force on the tip for further insertion of the guidewire in a tortuous path and comparison with the case of using no pulling force. (A, C, E, and F) The guidewire is further inserted by applying the magnetic pulling force on the tip (the locations shown are not the ultimate location of the insertion). **(B, D, G, and H)** The tip of the guidewire does not advance in the vessel without a magnetic pulling force, and the guidewire bends at its floppy distal section due to opposing forces from the vessel walls. The area inside the dashed line indicates the crooked part of the guidewire.

force applied on the tip to further insert the guidewire. The experiment was done by using the strong pulling force ($\nabla B > 2 \text{ T/m}$) and a weak pulling force ($\nabla B \in \{0.5 \text{ to } 1 \text{ T/m}\}$). The phantom was filled with water, and the guidewire used for the experiment had a hydrophobic coating. The tip of the guidewire was placed at each of the targets of the phantom, and the patient table was positioned to align the magnetic gradient force with the direction of the vessel. This experiment was done for targets 1, 2, 3, and 5; for all of them, long tortuous sections had to be passed to reach the targets.

In all cases, using a stronger pulling force helped to insert the guidewire further, whereas this was impossible when not using a pulling force (see Fig. 4 and supplementary movies). In addition, in one experiment, because the magnetic tip broke from the guidewire while the guidewire tip was at target 3, we observed that further insertion of a guidewire that had no magnetic tip was not possible. These results are evidence that the strong pulling force applied on the tip enables insertion of the guidewire further into the blood vessel, whereas the insertion of the guidewire from the other end is not effective for the advancement of the tip of the guidewire in vessels.

FFN in narrow vessels is demonstrated in vivo

We did in vivo FFN experiments in the neck and brain arteries of the swine animal model to navigate microguidewire with a magnetic

tip into branches of the common carotid artery (CCA). Two animals with weights of 25 and 24 kg were used for the experiments. All animals were treated humanely and according to the guidelines of the ethics committee of the University of Montréal.

For animal 1, FFN experiment was performed inside the left CCA. Because of the physiological feature of Rete Mirabile in swine (40), we chose the external carotid artery for the path of the navigation. In addition, this target required passing three branches to reach the target. The magnetic guidewire was fabricated by bonding a cylindrical neodymium permanent magnet with a length and a diameter of 1 mm to the tip of the same type of the microguidewire used in in vitro experiments. The microguidewire was placed retrogradely inside a microcatheter (FasTracker 18, Boston Scientific), and the composition was inserted into the 6-French catheter priorly placed inside the left CCA. The end of the microcatheter was fixed to the outlet of the guidewire feeder system, and intravenous fluid was administered into the microcatheter to reduce the friction between the microguidewire and the microcatheter. An x-ray image was taken at the beginning of the experiment, and the vascular trajectory was registered on it. The tip of the guidewire was placed inside the CCA at a location that corresponded to the initial point of the trajectory of the vessels deduced from the vascular registration on the x-ray image.

The selected path for FFN experiment was segmented, and sequences of navigation were defined for each segment. Sequential robotic positioning and insertion of the guidewire followed by a step of localization of the tip under x-ray were performed. For animal 1, the magnetic guidewire was successfully navigated to the selected target for the navigation. Figure 5 shows the x-ray image taken at the end of the experiment. In addition, the registration of the trajectory on the x-ray image was done *in vivo*, and its accuracy was evaluated by registration on a digital subtraction angiography image (see fig. S3). This registration was done before performing any FFN positioning with the spatial rotation of the animal. However, slight movement of the patient throughout the FFN intervention may occur due to the spatial rotation of the patient that can corrupt the registration accuracy. A method for correcting the registration of vascular trajectory is proposed here (see Supplementary Materials and Methods). We used it to correct the error in registration due to the movement of the animal, and the result is presented in fig. S3.

For animal model 2, the 6-French catheter was placed in the right CCA. The arteries of the catheterized side of the brain were invisible in MR angiography (Fig. 5). Therefore, trajectory planning and vascular registration were not possible. In this experiment, the animal was in the supine pose with its head straight. So we used the mirror of the arteries of the left side of the brain for defining the vascular trajectory. The vessel selected for the target of FFN was the ascending pharyngeal artery (APA), which is the first branch of the CCA. The diameter of APA was 2 mm on the left side of the brain of the animal. The guidewire was prepared by bonding a tubular neodymium permanent magnet with an inside diameter of 0.5 mm, an outside diameter of 1 mm, and a length of 1 mm. The volume of the magnetic tip used for the second *in vivo* experiment was 25% less than the volume of the tip used in the first animal model. The navigation to the APA was done by placing the tip of the magnetic microguidewire less than 1 cm before the bifurcation, moving the table to the position of the sequence of FFN, and inserting the guidewire 2 cm. Navigation into APA was done successfully and with repeatability (twice in a row without failure). The strength and the gradient of the magnetic field used for the navigation were about 0.6 T and more than 2 T/m, respectively. Figure 5 shows the results of the *in vivo* experiment on animal model 2.

The effect of the pulling force exerted on the tip for further insertion of the guidewire that was demonstrated *in vitro* was also validated in animal model 2. It was done by pulling the guidewire back to the beginning of the APA from the position the tip was placed at the end of FFN experiment (the tip is still inside the APA) and trying to insert the guidewire under fluoroscopy while the animal was far away from the MRI scanner ($B \sim 0.5$ mT). As a result, the insertion of the guidewire without using a pulling force on the tip was not possible, and the guidewire did not advance into APA (Fig. 6). We conclude that, for a microguidewire with a magnetic tip, a pulling force is necessary to insert the guidewire in a vessel when insertion of the guidewire is not possible.

Deformable spring as an alternative to solid permanent magnet tip

An important part of a catheter-based procedure is the retrieval of the guidewire. The solid permanent magnet tip limits the minimum size of the catheter used for a procedure. Although the possibility of the miniaturization of the permanent magnet tip is one solution, we also propose using a spring fabricated by winding a magnetic wire

for the tip. The high strength of the magnetic field available in FFN enables bringing the tip to its magnetic saturation state. The envisioned mechanisms for the deformation of the tip through the step of retrieving the guidewire are the spring tip that either bends or unwinds inside the catheter. We prepared a guidewire by bonding a spring to the microguidewire with an epoxy resin composition. The spring was fabricated by winding a deformable wire of stainless steel 430 with a diameter of 0.2 mm. We observed that, for a spring with a pitch distance equivalent to the diameter of the wire and when the ratio of the length to the diameter of the coil was larger than 2, it magnetized along its center axis at different zones in front of the MRI scanner (see movie S10). The spring that we fabricated for the tip of the guidewire had a length of ~ 2 mm and a diameter of ~ 0.7 mm. The vibrating sample magnetometer (VSM) test showed that the coil reached 95% of its magnetic saturation state when the strength of the external magnetic field was 0.5 T. We performed *in vitro* experiments by using the same map of the magnetic gradient force that we calculated for a permanent magnet tip, and the guidewire was navigated to targets 1, 3, 5, and 6 in our vascular model (see supplementary movies). We did not investigate the possibility of retrieving the guidewire because the material used for bonding the tip to the tether solidified the tip. Further explanation regarding this proposition and fabrication recommendations are provided in the next section.

DISCUSSION

In this work, we demonstrated that the idea of using a strong pulling force exerted on the tip of a soft guidewire is useful and effective to steer and insert the guidewire and to counteract the friction forces being amplified by the added surface in contact against the vessel walls caused by the bending of the instrument. Here, through *in vitro* and *in vivo* experiments, it is demonstrated that applying a pulling force on the tip of the microguidewire with a floppy distal enables further insertion of the instrument in the blood vessels as a way to reach to deeper anatomical regions. The use of the MRI fringe field for providing such a directional force within the body is also a way of leveraging the application of MRI scanners.

In FFN, the way the patient lays on the robotic table plays an important role because it changes the direction of the vessels. Different recumbent positions change the direction of the vessels on the patient table. It affects the efficiency of the FFN regarding the strength of the magnetic actuation because the magnetic force in FFN is mainly toward the MRI bore, and the pitch and roll rotation of the table have to be limited. Common abdominal endovascular interventions are performed in different branches of the aorta, and superselective catheterization aims to place the catheter deeper inside the vascular system. For each specific target in the abdomen, recumbent positions influence the efficiency of FFN. For instance, supine or prone positions can be the best position for navigation into the branches of renal arteries with FFN. For navigation into the branches of the celiac trunk or the superior mesenteric artery, the lateral recumbent positions may be preferred. For intervention inside the brain, turning and bending the neck also influences the efficacy of FFN. For intervention inside the legs, the proper positioning of the patient could require putting the head near the end effector while the legs are laying toward the other end of the table. To avoid underrepresenting the potential of FFN for specific endovascular intervention, we recommend case-specific studies to find the proper body position of the patient on the table for each

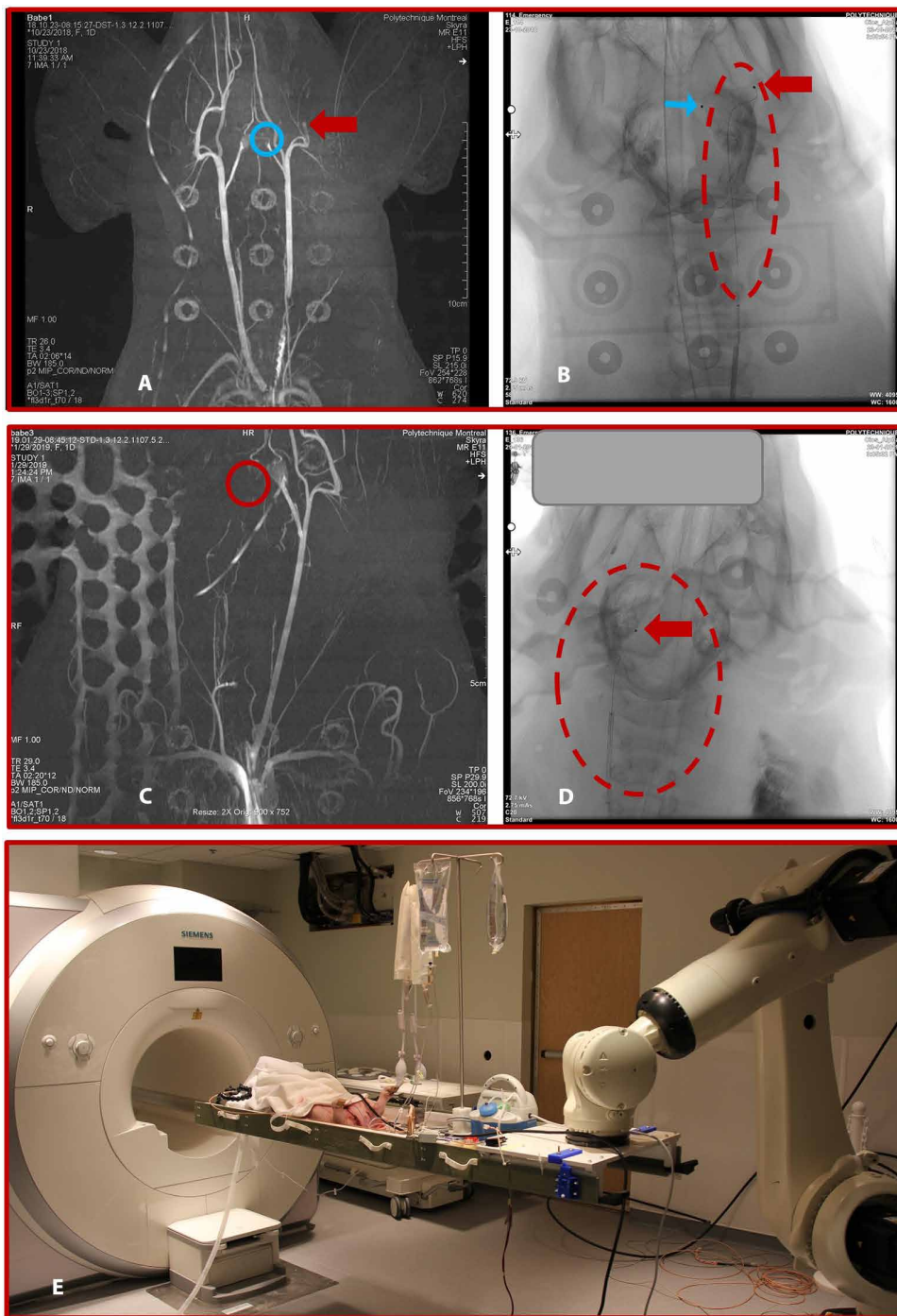


Fig. 5. Results of in vivo experiment of FFN. (A) and (B) are related to animal model 1 and (C) and (D) are related to animal model 2. The red arrow in (A) and red circle in (C) indicate the selected target in MRI angiography, and red arrows in (B) and (D) show the final location of the tip of the guidewire at the end of each experiment. Blue symbols in (A) and (B) show a magnet that is released from the tip of a guidewire to act as a fiducial marker and imaged by x-ray. (E) Animal placed on the patient table for an FFN experiment. The gray area in (D) is related to an instrument used for a different experiment.

intervention. By finding the range of available strengths and gradients of the magnetic field for specific interventions, these data, along with the diameter of the blood vessels at different anatomical regions, can be used for designing custom guidewires for FFN intervention.

To calculate the direction of the magnetic gradient force, the orientation of the tip of the guidewire inside the body needs to be known. The stiffness of the tether, the contact forces with the vessel walls, and blood flow speed can affect the orientation of the tip inside the blood vessels. In calculating the map of the magnetic gradient force, the direction of the tip of the guidewire is assumed to align with the external magnetic field. This assumption is made based on the following: (i) We used guidewires with floppy distal to reduce resistance against bending, and (ii) FFN uses a strong magnetic field (larger than 0.5 T). These assumptions were validated visually with a 3D magnetic probe throughout our experiments. In addition, in the experiments performed at $B \sim 0.15$ T, we observed that the tip still aligns with the external magnetic field. However, this assumption would not be correct in the case of using a stiffer catheter or a guidewire with a larger diameter. In such a case, using the pulling force would not be necessary because steering the device can be performed by applying torque on the tip of the instrument, as demonstrated in previous works (7, 22, 25–27).

An important factor regarding FFN is the required time to perform a procedure. Each sequence of robotic positioning of the patient for navigation took about 1 to 2 min to transport the patient to the target position from a general position. This transportation was executed with limited velocity and acceleration to allow very smooth displacement of the patient table. FFN is proposed for performing selective steering of the guidewire at bifurcations and to insert the guidewire in narrow blood vessels by applying a pulling force on the tip. A way to optimize the time of an intervention is to limit performing FFN sequences to challenging parts of the vascular system where the magnetic actuation from the fringe field is essential. In addition, the slowness of the physical movement of the patient in FFN makes it an inappropriate tool for operation inside the heart, which has fast dynamics.

The method of vascular registration developed here does not account for the deformation of the organs. In FFN, respiration, cardiac function, and gravity can deform the internal organs, leading to the inaccuracy of the trajectory of the vessel. This inaccuracy induces error in the 6-DOF positioning of the patient inside the map of the fringe field



Fig. 6. Two examples of failure in the insertion of the guidewire in APA without a pulling force on the tip. The gray areas in (A) and (B) are related to an instrument used for a different experiment.

as well as the registration of the vascular trajectory. Further development is required to develop a registration method that takes into account the deformations of the internal organs. However, respiratory gating and proper immobilization of the patient could help to reduce the impact of the displacements for an FFN intervention. In addition, image guiding of the intervention by fluoroscopy is a safe way of guiding the intervention.

Operating an industrial robot near an MRI would raise concerns regarding the safety. In this work, the operating zone of the robot was limited to a space where the strength of the magnetic fringe field was less than 20 mT. The fringe field applies force and torque on the magnetic parts of the robot, which leads to an increase in the load on the drivers of the robot. Although the experiments performed were shown to be safe, more investigations could be done to validate further an optimal safe working space for the operation of the robot near an MRI scanner.

The possibility of using a deformable magnetic tip enhances the potential of a catheter-based procedure by facilitating the step of guidewire retrieval. Here, we proposed and validated *in vitro* navigation of a microguidewire by the use of a spring-shaped tip. Among all the systems developed for magnetic navigation, FFN features a uniquely high strength of magnetic field that brings such a tip to the saturation level (22). One remaining aspect to be investigated is the method of bonding the coil to the tether to enable retrieval of the guidewire. Dissimilar welding followed by heat treatment can be a method of fabrication to attach NiTi wire as the tether to a coil made of stainless steel (41). Optimization of the diameter of the wire and dimensions of the coil is required for success of retrieval. We consider the design, optimization, and fabrication of such a guidewire as future work.

Conclusion

The fringe field has been used for steering and insertion of a guidewire at a remote location inside the vessels by applying a pulling force on the tip. This outcome allows targeting vessels for endovascular intervention in a robotic manner independent of the experience of the interventionist. Stronger actuation in FFN also allows miniaturization of the tip as a way to enable targeting narrower blood vessels. Successful implementation of the FFN protocol for robotic catheterization in an *in vivo* experiment and navigation of the guidewire demonstrates the potential of FFN for catheter-based procedures. In addition, FFN as a robotic approach brings task autonomy to performing endovascular catheterization, which presently highly depends on the experience of the physician. FFN has the high potential to navigate microguidewires in narrow blood vessels throughout multiple bifurcations.

MATERIALS AND METHODS

Mapping the fringe field

On the basis of the data provided by the manufacturer of the MRI scanner, the lines of the magnetic fringe field are distributed axisymmetrically about the center axis of the MRI tunnel. We verified this by probing the direction of the magnetic field lines in front of the MRI scanner. Mapping the magnetic field was done by sampling a radial plane of the fringe field. We used a three-axis probe with a resolution of 0.1 mT (F3A-3MH3A, Senis, Switzerland), which we mounted on a specific tool attached to the end effector of the robotic manipulator to measure the components of the magnetic field. The positioning accuracy of the robotic system was 60 μm . The height of the center axis of the MRI was found by measuring the component

of the magnetic field perpendicular to the radial plane parallel to the floor of the venue. The height of this plan was found with less than 0.5-cm error, and the mean value for this component of the magnetic field for all the sampled points was 1 mT (ranging between -4 and $+4$ mT). Then, the axial and radial components of the fringe field were measured at different points. We took 800 samples at a distance of 1.5 m in the radial direction and 1.2 m in the axial direction from the center axis and front face of the MRI as well as inside the MRI tunnel.

Thin-plate spline interpolation (42, 43) was used to calculate the strength of the magnetic field at any arbitrary point in the radial plane of the fringe field. The accuracy of the interpolation was investigated for the points at which the strength of the magnetic field is above 0.4 T. It was done by interpolating the components of the strength of the field at each point by using all collected data except data collected from that point and comparing the result of the interpolation with the measurement. The average errors of the interpolation for the radial and axial components of the magnetic field were 0.0032 and 0.0022 T with variances of 6.61×10^{-6} and 4.13×10^{-6} , respectively. The 3D map of the fringe field was produced from the radial map of the fringe field. The direction of the magnetic gradient force applied on a magnetic body is a function of its magnetic moment and the partial derivative of the components of the magnetic field (Jacobian) (44). The Jacobian matrix of the magnetic field was calculated by the interpolation and differentiation of each component of the magnetic field along the different axes in 3D space. Then, the map of the direction of the magnetic gradient force was produced by assuming that the magnetic moment of the tip can align itself with the external magnetic field.

Animal preparation for in vivo experiments

The protocol of the experiment was approved by the ethics committee of the University of Montréal. The animal model was a farm breed swine. The same patient table used in in vitro experiments was used for this experiment. The pole for the intravenous unit was installed at the end of the table onto a holder made of nylon and moved with the table during robotic positioning. The preparation of each animal was done under general anesthesia. Vascular access was made in the femoral artery. A 6-French catheter (Guider Softip XF, Boston Scientific) was placed into the CCA. After finishing the catheterization, the animal was put in the supine position on the table and immobilized by the use of straps to limit its movement throughout the FFN experiment.

Before the beginning of the experiment, the grid of fiducial markers was fixed on the table. Multimodality markers were used for referencing the vascular trajectory on the patient table, calibration, and vessel registration. The location of the markers was chosen in a way to be visible in field of view (FOV) of MRI angiography of the neck and brain as well as FOV of the x-ray. After selective catheterization of the CCA, the animal was immobilized on the table and transferred to the MRI for angiography of the neck and the brain. Phase contrast MRI imaging sequence was used for angiography. The imaging parameters were repetition time (TR) = 29 ms and echo time (TE) = 3.4 ms, and the size of the voxel was 0.25 mm by 0.25 mm by 0.5 mm. After MRI angiography, the table was mounted on the robot and was moved to the x-ray for imaging, registration, and determination of the required position for the magnetic guidewire at the beginning of the experiment.

SUPPLEMENTARY MATERIALS

robotics.sciencemag.org/cgi/content/full/4/36/eaax7342/DC1

Materials and Methods

- Fig. S1. Multiple views of the 3D model of the vascular phantom used in in vitro experiments.
 Fig. S2. In vitro results of registration of vessel centerline.
 Fig. S3. Registration of the vascular trajectory on the x-ray image.
 Fig. S4. Example of planning vascular trajectory and its segmentation to plan FFN experiment.
 Fig. S5. The order of the fringe field map from the best points for navigation to the least appropriate points.
 Fig. S6. The working zones for the robotic patient positioning.
 Fig. S7. Pictures of robotic positioning of the patient table.
 Movie S1. In vitro: Targets 1 and 2 and the retrieval of the guidewire.
 Movie S2. In vitro FFN: Navigation to target 3 and trying to insert the device without FFN.
 Movie S3. In vitro FFN: Target 4 and retrieval of the guidewire.
 Movie S4. In vitro FFN: Target 5 and retrieval of the guidewire.
 Movie S5. In vitro FFN: Target 6.
 Movie S6. In vitro FFN: Demonstration of the strong magnetic actuation in FFN for navigation.
 Movie S7. In vitro FFN: Further insertion of the guidewire by exerting a gradient pulling force on the tip of the guidewire.
 Movie S8. In vitro FFN: Further insertion of the guidewire by exerting a gradient pulling force on the tip of the guidewire.
 Movie S9. In vitro FFN: Further insertion of the guidewire by exerting a gradient pulling force on the tip of the guidewire.
 Movie S10. Interaction between a spring and the magnetic field.
 Movie S11. Navigation of a guidewire with a spring magnetic tip.
 Movie S12. Navigation of a guidewire with a spring magnetic tip.
 Movie S13. Navigation of a guidewire with a spring magnetic tip.
 Movie S14. Navigation of a guidewire with a spring magnetic tip.
 Reference (45)

REFERENCES AND NOTES

1. P. Song, D. Rudan, Y. Zhu, F. Fowkes, K. Rahimi, G. Fowkes, I. Rudan, Global, regional, and national prevalence and risk factors for peripheral artery disease in 2015: An updated systematic review and analysis. *Lancet* **7**, e1020–e1030 (2019).
2. F. Bray, J. Ferlay, I. Soerjomataram, R. Siegel, L. Torre, A. Jemal, Global cancer statistics 2018: GLOBOCAN estimates of incidence and mortality worldwide for 36 cancers in 185 countries. *CA Cancer J. Clin.* **68**, 394–424 (2018).
3. A. Adam, L. Kenny, Interventional oncology in multidisciplinary cancer treatment in the 21st century. *Nat. Rev. Clin. Oncol.* **12**, 105–113 (2015).
4. B. J. Nelson, I. K. Kaliakatsos, J. J. Abbott, Microrobots for minimally invasive medicine. *Annu. Rev. Biomed. Eng.* **12**, 55–58 (2010).
5. J. Bonatti, G. Vetrovecc, C. Riga, O. Wazni, P. Stadler, Robotic technology in cardiovascular medicine. *Nat. Rev. Cardiol.* **11**, 266–275 (2014).
6. H. W. Huang, F. E. Uslu, P. Katsamba, E. Lauga, M. S. Sakar, B. J. Nelson, Adaptive locomotion of artificial microswimmers. *Sci. Adv.* **5**, eaau1532 (2019).
7. L. Ricotti, B. Trimmer, A. W. Feinberg, R. Raman, K. K. Parker, R. Bashir, M. Sitti, S. Martel, P. Dario, A. Mencias, Biohybrid actuators for robotics: A review of devices actuated by living cells. *Sci. Robot.* **2**, eaq0495 (2017).
8. S. Jeon, S. Kim, S. Ha, S. Lee, E. Kim, S. Y. Kim, S. H. Park, J. H. Jeon, S. W. Kim, C. Moon, B. J. Nelson, J.-y. Kim, S.-W. Yu, H. Choi, Magnetically actuated microrobots as a platform for stem cell transplantation. *Sci. Robot.* **4**, eaav4317 (2019).
9. O. Felfoul, M. Mohammadi, S. Taherkhani, D. de Lanauze, Y. Z. Xu, D. Loghin, S. Essa, S. Jancik, D. Houle, M. Lafleur, L. Gaboury, M. Tabrizian, N. Kaou, M. Atkin, T. Vuong, G. Batist, N. Beauchemin, D. Radzioch, S. Martel, Magneto-aerotoxic bacteria deliver drug-containing nanoliposomes to tumour hypoxic regions. *Nat. Nanotechnol.* **11**, 941–947 (2016).
10. J. Li, B. Esteban-Fernández de Ávila, W. Gao, L. Zhang, J. Wang, Micro/nanorobots for biomedicine: Delivery, surgery, sensing, and detoxification. *Sci. Robot.* **2**, eaam6431 (2017).
11. S. Martel, Beyond imaging: Macro- and microscale medical robots actuated by clinical MRI scanners. *Sci. Robot.* **2**, eaam8119 (2017).
12. X. Yan, Q. Zhou, M. Vincent, Y. Deng, J. Yu, J. Xu, T. Xu, T. Tang, L. Bian, Y.-X. J. Wang, K. Kostarelos, L. Zhang, Multifunctional biohybrid magnetite microrobots for imaging-guided therapy. *Sci. Robot.* **2**, eaq1155 (2017).
13. M. Sitti, Miniature soft robots—Road to the clinic. *Nat. Rev. Mater.* **3**, 74–75 (2018).
14. G. Z. Yang, J. Bellingham, P. E. Dupont, P. Fischer, L. Floridi, R. Full, N. Jacobstein, V. Kumar, M. McNutt, R. Merrifield, B. J. Nelson, B. Scassellati, M. Taddeo, R. Taylor, M. Veloso, Z. L. Wang, R. Wood, The grand challenges of *Science Robotics*. *Sci. Robot.* **3**, eaar7650 (2018).
15. S. N. Tabatabaei, H. Girouard, A. Carret, S. Martel, Remote control of the permeability of the blood–brain barrier by magnetic heating of nanoparticles: A proof of concept for brain drug delivery. *J. Control. Release* **209**, 49–57 (2015).

16. A. Roguin, J. Goldstein, O. Bar, J. A. Goldstein, Brain and neck tumors among physicians performing interventional procedures. *Am. J. Cardiol.* **111**, 1368–1372 (2012).
17. E. Vano, N. J. Kleiman, A. Duran, M. Romano-Miller, M. M. Rehani, Radiation-associated lens opacities in catheterization personnel: Results of a survey and direct assessments. *J. Vasc. Interv. Radiol.* **24**, 197–204 (2013).
18. D. Alexandre, M. Prieto, F. Beaumont, R. Taiar, G. Polidori, Wearing lead aprons in surgical operating rooms: Ergonomic injuries evidenced by infrared thermography. *J. Surg. Res.* **209**, 227–233 (2017).
19. P. Schneider, *Endovascular Skills: Guidewire and Catheter Skills for Endovascular Surgery* (CRC Press, ed. 3, 2008).
20. C. D. Owens, Y. Yeghiazarians, *Handbook of Endovascular Peripheral Interventions* (Springer Science & Business Media, 2011).
21. G.-Z. Yang, J. Cambias, K. Cleary, E. Daimler, J. Drake, P. E. Dupont, N. Hata, P. Kazanzides, S. Martel, R. V. Patel, V. J. Santos, R. H. Taylor, Medical robotics—Regulatory, ethical, and legal considerations for increasing levels of autonomy. *Sci. Robot.* **2**, eaam8638 (2017).
22. N. Shamsudhin, V. I. Zverev, H. Keller, S. Pane, P. W. Egolf, B. J. Nelson, A. M. Tishin, Magnetically guided capsule endoscopy. *Med. Phys.* **44**, e91–e111 (2017).
23. H. Rafii-Tari, C. J. Payne, G.-Z. Yang, Current and emerging robot-assisted endovascular catheterization technologies: A review. *Ann. Biomed. Eng.* **42**, 697–715 (2014).
24. V. Vitiello, S.-L. Lee, T. P. Cundy, G.-Z. Yang, Emerging robotic platforms for minimally invasive surgery. *IEEE Rev. Biomed. Eng.* **6**, 697–715 (2013).
25. G. A. Antoniou, C. V. Riga, E. K. Mayer, N. J. W. Cheshire, C. D. Bicknell, Clinical applications of robotic technology in vascular and endovascular surgery. *J. Vasc. Surg.* **53**, 493–499 (2011).
26. S. Ramcharitar, M. S. Patterson, R. J. V. Geuns, C. V. Meighem, P. W. Serruys, Technology insight: Magnetic navigation in coronary interventions. *Nat. Clin. Pract. Cardiovasc. Med.* **5**, 148–156 (2008).
27. A. Ali, D. H. Plettenburg, P. Breedveld, Steerable catheters in cardiology: Classifying steerability and assessing future challenges. *IEEE Trans. Biomed. Eng.* **63**, 679–693 (2016).
28. F. Carpi, C. Pappone, Stereotaxis Niobe[®] magnetic navigation system for endocardial catheter ablation and gastrointestinal capsule endoscopy. *Expert Rev. Med. Devices* **6**, 487–498 (2009).
29. M. P. Kummer, J. J. Abbott, B. E. Kratochvil, R. Rorer, A. Sengul, B. J. Nelson, OctoMag: An electromagnetic system for 5-DOF wireless micromanipulation. *IEEE Trans. Robot.* **26**, 1006–1017 (2010).
30. E. S. Gang, B. L. Nguyen, Y. Shachar, L. Farkas, L. Farkas, B. Marx, D. Johnson, M. C. Fishbein, C. Gaudio, S. J. Kim, Dynamically shaped magnetic fields: Initial animal validation of a new remote electrophysiology catheter guidance and control system. *Circ. Arrhythm. Electrophysiol.* **4**, 770–777 (2011).
31. I. Tunay, S.-Y. Yoon, K. Woerner, R. Viswanathan, Vibration analysis and control of magnet positioner using curved-beam models. *IEEE Trans. Control Syst. Technol.* **17**, 1415–1423 (2009).
32. I. Tunay, Spatial continuum models of rods undergoing large deformation and inflation. *IEEE Trans. Robot.* **29**, 297–307 (2013).
33. S. Jeon, A. K. Hoshiar, K. Kim, S. Lee, E. Kim, S. Lee, J.-Y. Kim, B. J. Nelson, H.-J. Cha, B.-J. Yi, H. Choi, A magnetically controlled soft Microrobot steering a guidewire in a three-dimensional phantom vascular network. *Soft Robot.* **6**, 54–68 (2018).
34. J. Edelmann, A. J. Petruska, B. J. Nelson, Magnetic control of continuum devices. *Int. J. Rob. Res.* **36**, 68–85 (2017).
35. V. N. Le, N. H. Nguyen, K. Alameh, R. Weerasooriya, P. Pratten, Accurate modeling and positioning of a magnetically controlled catheter tip. *Med. Phys.* **43**, 650–663 (2016).
36. V. Lalonde, F. P. Gosselin, M. Vonthron, B. Conan, C. C. Tremblay, G. Beaudoin, G. Soulez, S. Martel, In vivo demonstration of magnetic guidewire steerability in a MRI system with additional gradient coils. *Med. Phys.* **42**, 969–976 (2015).
37. C. C. Tremblay, B. Conan, D. Loghin, A. Bigot, S. Martel, Fringe field navigation for catheterization, in *Proceedings of the 6th European Conference of the International Federation for Medical and Biological Engineering*, Dubrovnik, Croatia, 7 to 11 September 2014, pp. 379–382.
38. Y. Kim, G. A. Parada, S. Liu, X. Zhao, Ferromagnetic soft continuum robots. *Sci. Robot.* **4**, eaax7329 (2019).
39. D. W. McRobbie, Occupational exposure in MRI. *Br. J. Radiol.* **85**, 293–312 (2012).
40. M. M. Swindle, A. C. Smith. *Swine in the Laboratory: Surgery, Anesthesia, Imaging, and Experimental Techniques* (CRC Press, ed. 3, 2015).
41. J. P. Oliveira, R. M. Miranda, F. M. B. Fernandes, Welding and joining of NiTi shape memory alloys: A review. *Prog. Mater. Sci.* **88**, 412–466 (2017).
42. S. C. Chapra, R. P. Canale, *Numerical Methods for Engineers* (McGraw-Hill Higher Education, 2010).
43. A. Azizi, C. C. Tremblay, S. Martel, Magnetic fringe field navigation of a guidewire based on Thin Plate Spline modeling, in *Proceedings of the 2016 IEEE International Conference on Automation Science and Engineering*, Fort worth, TX, 21 to 24 August 2016, pp. 567–572.
44. J. J. Abbott, O. Ergeneman, M. P. Kummer, A. M. Hirt, B. J. Nelson, Modeling magnetic torque and force for controlled manipulation of soft-magnetic bodies. *IEEE Trans. Robot.* **23**, 1247–1252 (2007).
45. A. Azizi, C. C. Tremblay, S. Martel, Trajectory planning for vascular navigation from 3D angiography images and vessel centerline data, in *Proceedings of the IEEE International Conference on Manipulation, Automation and Robotics at Small Scales*, Montreal, QC, 17 to 21 July 2017, pp. 1–6.

Acknowledgments: We thank S. Ménard for support in conducting the animal experiments, preparation of the animals, and performing the catheterization. We thank D. Ménard and D. Seddaoui for performing the VSM tests. In addition, we thank D. Loghin for support in the development of the software for the communication with the robot. **Author contributions:** S.M. developed the concept of FFN and acted as the principal investigator of the project. A.A., C.C.T., and S.M. worked on the method of navigation with FFN. A.A. and C.C.T. worked on the design and fabrication of the magnetic microguidewire and patient table. A.A. performed in vitro experiments. A.A., K.G., and C.C.T. worked on the strategy of collision avoidance and patient positioning. K.G., A.A., and C.C.T. worked on developing the software for communication with the robot. C.C.T. developed the MRI and x-ray protocols. A.A., C.C.T., K.G., and S.M. worked on developing the protocol of in vivo experiment. A.A. wrote the manuscript, and S.M., C.C.T., and K.G. revised the manuscript. **Competing interests:** The authors declare that they have no competing interests. **Data and materials availability:** All data needed to evaluate the conclusions in the paper are present in the paper or the Supplementary Materials.

Submitted 4 July 2019
 Accepted 29 October 2019
 Published 27 November 2019
 10.1126/scirobotics.aax7342

Citation: A. Azizi, C. C. Tremblay, K. Gagné, S. Martel, Using the fringe field of a clinical MRI scanner enables robotic navigation of tethered instruments in deeper vascular regions. *Sci. Robot.* **4**, eaax7342 (2019).

Using the fringe field of a clinical MRI scanner enables robotic navigation of tethered instruments in deeper vascular regions

Arash Azizi, Charles C. Tremblay, Kévin Gagné, and Sylvain Martel

Sci. Robot. **4** (36), eaax7342. DOI: 10.1126/scirobotics.aax7342

View the article online

<https://www.science.org/doi/10.1126/scirobotics.aax7342>

Permissions

<https://www.science.org/help/reprints-and-permissions>

Use of this article is subject to the [Terms of service](#)

Science Robotics (ISSN 2470-9476) is published by the American Association for the Advancement of Science, 1200 New York Avenue NW, Washington, DC 20005. The title *Science Robotics* is a registered trademark of AAAS.

Copyright © 2019 The Authors, some rights reserved; exclusive licensee American Association for the Advancement of Science. No claim to original U.S. Government Works